MSc Quantum Science and Technology

Master Thesis

Quantum State Transfer with Ising Hamiltonians

Author: Oscar Michel González

Supervised by: Matthias Werner, Arnau Riera

NIUB: 20102832
Faculty of Physics, University of Barcelona
08028, Barcelona
July 6th 2025

Acknowledgements

I would first like to thank my two supervisors Matthias Werner and Arnau Riera for their invaluable help throughout the whole project, the frequent meetings in which we discussed ideas and overcame difficulties, and their overall interest and dedication to this thesis. I extend the gratitude to the entire team of Qilimanjaro that made me feel at home from day one and gave me the perfect environment and resources in which to learn about quantum computing and develop a strong project.

Secondly, I thank the Catalonia Quantum Academy for their support during the internship with a Student Mobility Fellowship, which allowed me to acquire experience outside the university and dedicate myself fully to the research.

Next, to my friends from the master's in quantum science and technology, Ángel, Berkant, Raven, Joan, and Super Julie, for the countless hours of joint study in the library, their emotional support, and for filling this past year with laughs and good memories.

Finally to my family, ever-present in my mind, that has become my anchor in the long and winding path that is academia.

And to Yara. Always to Yara.

Abstract

Quantum state transfer is a fundamental requirement for scalable quantum computation, where fast, reliable communication between distant qubits is essential. In this work, we present a protocol for quantum state transfer in linear spin chains tailored to superconducting flux qubits. Starting from a perfect state transfer scheme via a Heisenberg Hamiltonian with inhomogeneous couplings [CDEL04], we adapt it to superconducting architectures by encoding the information in domain walls. The resulting Hamiltonian only contains ZZ interactions, allowing us to produce quantum transport in superconducting devices constrained to Ising-like couplings. We test the protocol for 1-, 2-, and 3- qubit states, obtaining high transfer fidelities of up to 0.99, and study the accuracy dependence on the domain wall approximation. Additionally, we analyze the protocol's robustness to hardware errors, and determine tolerances to 7% variations in the transverse X fields, 0.9% in the coupling strengths, and up to 3MHz in local Z perturbations. Finally, we estimate the parameters required for a fluxonium qubit [MKGD09] to effectively run our algorithm, paving the way for an experimental implementation of the protocol.

Contents

1 Introduction

Quantum computation and its applications have in recent years become an area of great interest for researchers and industry. Advances in superconducting technologies, optics, and control electronics have enabled the utilization of quantum systems to carry out logical operations [Llo96, Sho94, Gro96] and simulate complex phenomena [ZFRC17, BSK+17]. Simultaneously, a multitude of applications have been found where quantum computers can confer an advantage over classical computation [BV97, KEA+23, AAB+19]. Several platforms have emerged as candidates for a universal quantum computer. Among them are superconducting circuits [KYG+07, BDG+22], photonic integrated circuits [KLM01, YCY+25], trapped ions [CZ95, HRB08], and neutral atoms [JCZ+00, WDE+23]. Additionally, there is not a unique computational paradigm that to perform operations with quantum systems. The most widely known is gate-based quantum computing [NC10], which is the preferred scheme for most industrial applications for its versatility to encode and execute any type of quantum algorithm. Alternative computational paradigms include Measurement-based quantum computing [RB01, BBD+09], and Analog Quantum Computing [FGGS00, AL18], the latter being the target strategy of this thesis.

Analog Quantum Computing (AQC) aims to solve device-specific problems by encoding the properties of a quantum system –namely its Hamiltonian– in a physical device whose properties are suitable for simulating the target problem. Then, from the time evolution of the device we can find the solution to the original problem. There are several strategies to evolve these Hamiltonians, such as the ones involving the adiabatic theorem [BF28], by which a system in the ground state of a gapped Hamiltonian will remain in the ground state if the Hamiltonian is evolved sufficiently slowly [1]. The main advantage of AQC is that certain problems can easily be modeled by the kind of Hamiltonians that are natural to the computing platform [RGL+14, ZYL+25], allowing for an efficient solution in a quantum simulator.

The two main platforms where AQC has been implemented are neutral atoms [GB17], and superconducting circuits [YRS+22], the latter being of particular interest for industrial applications for the required manufacturing processes and flexibility in qubit connectivity and control. This is the platform in which we will focus for our study. The core idea behind analog superconducting processors is to create qubits where the superposition of ground state and first excited state can be evolved continuously by tuning the circuit currents and external fields [OMT+99, HP25]. This allows to encode an initial state into the qubit array, and evolve it continuously towards a final state, containing the solution to a particular problem. Flux qubits [LN24] are usually employed for this tasks. They are realized by using several Josephson Junctions or other inductors in a superconducting loop, as opposed to a single junction in regular Transmons. [KYG+07]. This allows the precise tuning of the Hamiltonian encoded in it via external fields. Example applications with these systems include the simulation of condensed matter systems [KSR+22, KS18], optimization problems [DC08, LPQ+22], and quantum machine learning [KHZ+24].

Another particular problem of interest is that of quantum transport [OL04]. The core objective of a transport protocol is to transfer a state across a certain distance with as high fidelity as possible. The simulation of this phenomenon requires a many-body system which in classical computation becomes exponentially large to simulate. Simulating quantum transport in analog devices can allow the study of long-range communication and multipartite state transfer in chains of qubits, applicable to problems such as intra-processor information transfer [ZHY+14], long-range quantum communications [KBDGL19], and

[1] "Slowly" means that for a given energy gap Δ the timescale of the evolution should be larger than $1/\Delta^2$.

quantum metrology [MLK+16]. The importance for understanding these protocols also applies to the research in quantum computing itself, since one of its many challenges is the communication between distant parts of a qubit array. Therefore, it is key to seek perfect state transfer independently of the distance.

Implementing state transport in hardware poses both technical and theoretical difficulties, and many proposals exist to create protocols of efficient and realizable quantum transport. Additionally, a simple state transfer protocol can be used as a benchmark test for small devices to measure their accuracy in quantum simulation, the level of control over individual qubits, and the errors introduced by hardware defects. It is then very relevant to determine which transport schemes work best in different devices by simulating the phenomenon in analog superconducting chips.

This is precisely the goal of this project, where we explore strategies to implement quantum transport in superconducting flux qubits. The main limitation of these protocols is given by the hardware, which in this case restricts us to modeling an Ising-like system with a transverse field [ODS+20, HPJPGR22]. This is in principle a big limitation since most transfer protocols work with Heisenberg Hamiltonians and involve interactions not yet available in superconducting devices. However, the choice of information encoding can expand the range of systems that we can recreate. In particular, we will perform simulations of quantum transport algorithms using a domain wall encoding [Cha19], which will allow us to overcome some of the hardware restrictions and simulate interactions beyond the ZZ term. With this strategy we aim to achieve single-qubit, and multi-qubit state transfer, as well as study the robustness of the method to errors, and the feasibility to be implemented in superconducting hardware. The content of this text will be structured as follows: Section 2 introduces the problem of quantum state transfer in more detail, as well as the original strategy by Christiandl et al. [CDEL04] that we have based our protocol on. Section 3 describes the adaptation we have made to implement the protocol with domain walls and give examples of state transfer with this strategy. Finally, Section 4 analyzes the precision of the domain wall approximation, and studies the hardware feasibility of our protocol and its robustness to different sources of errors, before ending with the conclusions and possible extensions.

2 State transfer in linear chains

2.1 State transfer basics

In this thesis we will simulate quantum state transfer along one-dimensional chains of spin-1/2 particles. The basics of the transfer process are as follows. We start with a chain of N spins all in the state $|0\rangle$, and we prepare a spin in one of the ends in a superposition $|\psi\rangle_1 (t=0) = \alpha|1\rangle + \beta|0\rangle$ [2]. Later we will prepare multi-qubit states but for simplicity we stick to the one-qubit case in this explanation. The transfer process consists of applying a given Hamiltonian to the chain and it through time. Then we consider that the state has been successfully transferred when at a certain time τ all the chain is in the state $|0\rangle$, except for the last spin, which now is in the same state as the first spin at time $t = 0$, $|\psi\rangle_N (\tau) = |\psi\rangle_1 (0) = \alpha|1\rangle + \beta|0\rangle$. A visual representation of this process can be seen in Figure 1

The main complication of this process is the choice of Hamiltonian, since we require very specific conditions for the state transfer to be successful. Over the years, several candidates

[2] In a chain of spins arranged from left to right, we will encode the state in the leftmost spin, and will refer to it as the first spin in the chain.

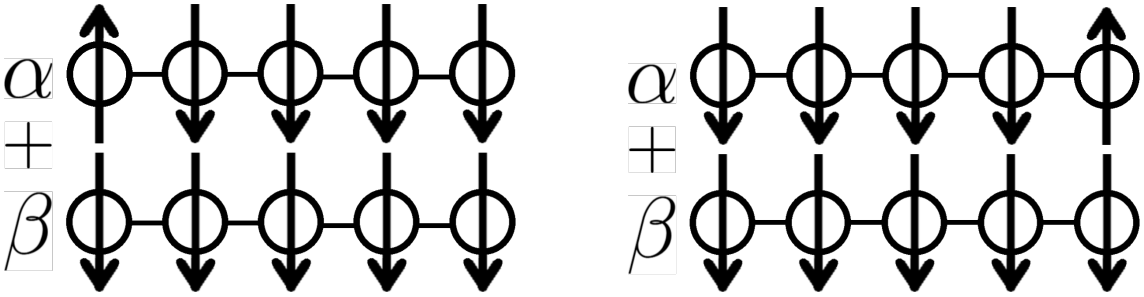

Figure 1: Schematic representation of the initial state (left) and final state (right) of the transport process of $|\psi\rangle = \alpha|1\rangle + \beta|0\rangle$ along an example chain of 5 qubits.

have emerged, each with its own advantages and drawbacks. We can summarise the most important characteristics for a transfer protocol as:

- To be as close to perfect as possible (fidelity 1 between the states at the ends of the chain)
- To work at arbitrary distances
- Preferably, the Hamiltonian should be as simple as possible and easily implementable in experiments

The first efforts to design state transfer protocols for quantum computing were done by S. Bose et al. [Bos03, Bur07]. The simplest version consists of a one-dimensional spin chain with a Heisenberg Hamiltonian and constant uniform couplings between Nearest-Neighbour spins

$$H = -J \sum_{<i,j>} \vec{\sigma^i} \cdot \vec{\sigma^j} - B \sum_{i=1}^{N} \sigma_z^i. \tag{1}$$

This system can transfer a state from the first spin to the last with fidelity 1 when $N \leq 4$, but for longer chains the fidelity decreases as $N^{-1/3}$. After that, several strategies appeared to keep the fidelity at 1, all involving modifications to the couplings or the system's geometry. These strategies include using time-dependent couplings [HKC+18], multiple chains [BB05], or "holes" at the ends [GMT09, WLK+05]. But at the same time, they pose challenges that can make it difficult to implement on hardware. In the case of superconducting qubits, not all platforms are capable of simulating time-dependent couplings, and chain holes require very small and chain-length-dependent couplings. However, one possible strategy is to use constant, but inhomogeneous couplings along the whole chain, such as in [CDEL04], which is the model in which we will base our protocol. In this case, they employ a XY Heisenberg Hamiltonian of the form

$$H_G = -\sum_{n=1}^{N-1} \frac{t_n}{2} \left[\sigma_n^x \sigma_{n+1}^x + \sigma_n^y \sigma_{n+1}^y\right]. \tag{2}$$

With a mirror symmetry in the coupling strengths such that

$$t_n = \frac{\lambda}{2}\sqrt{n(N-n)}. \tag{3}$$

This makes the Hamiltonian identical to the angular momentum operator of a spin $S = \frac{1}{2}(N-1)$ particle, $H = \lambda S_x$.

Under the Hamiltonian above, probability amplitude of state transport between the two ends of the chain is periodic in time,

$$\langle 00...01 | \, e^{-iH_G t} \, |10...00\rangle = \left[-i \sin\left(\frac{\lambda t}{2}\right)\right]^{N-1}. \tag{4}$$

So perfect state transfer can be achieved in $t = \pi/\lambda$ for any chain length. Note that this time is constant for any length of the chain N. This appears to be in contradiction with the intuition that any propagating effect must take longer to traverse a bigger system. However in this case the coupling strengths t_n also scale with the total qubit number N, meaning that the interactions are stronger for longer chains, and accelerate the transport velocity.

Additionally, the Hamiltonian above commutes with the total angular momentum operator $Z = \sum_{i=1}^{N} \sigma_z^i$, meaning that it conserves the number of excitations, i.e. number of spins in state $|1\rangle$. This property will be relevant when we make modifications to this initial protocol. Figure 1. shows an example of how the state $|1\rangle$ is transferred for a chain length of $N = 13$. We use two methods to visualize the results. One is by directly calculating the fidelity between the entire chain state at time t and the expected final state, as can be seen in Figure 2 (a). In the second one we plot the expectation value of the z-component of the spin $\langle \hat{Z} \rangle$, for each spin in the chain and each time step. This is a good visual way to see the state being transported, although for more complex states will not give as much information as the fidelity test.

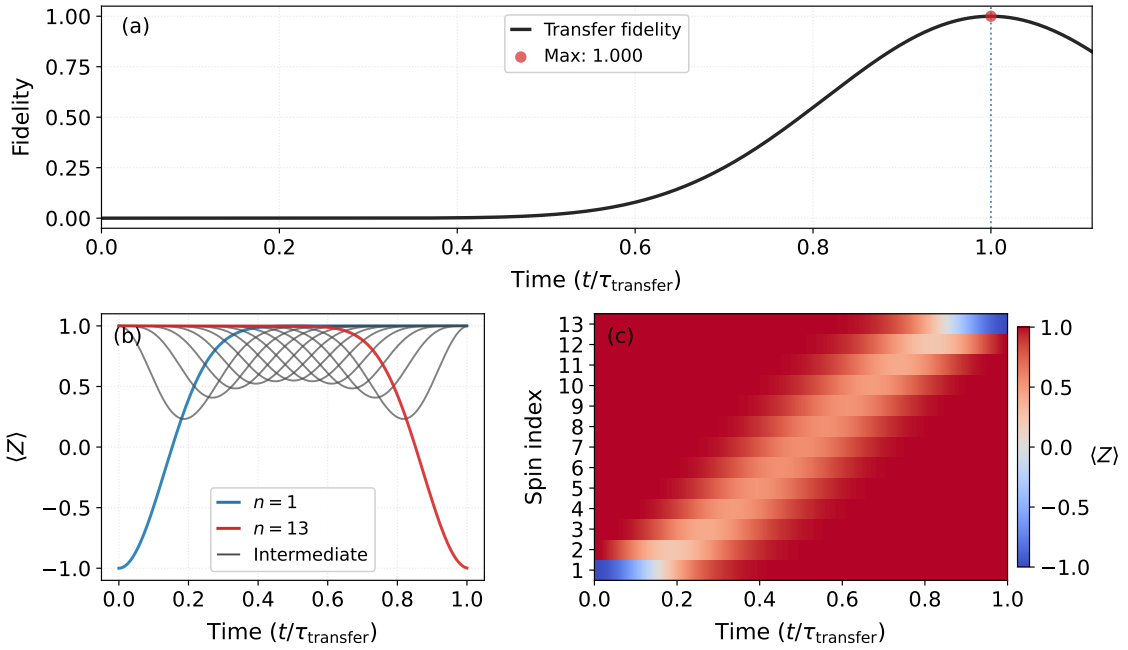

Figure 2: (a) Fidelity between the state at time t and the final expected state $|0...01\rangle$, for $N = 13$, and initial state $|10...0\rangle$. It reaches the maximum of 1 after a finite time τ_{transfer}. (b) Evolution of z-component of each spin. The -1 value corresponds to the spin in the $|1\rangle$ state, and the $+1$ to the state $|0\rangle$. We can observe the swap of the initial and final spins after time τ_{transfer}. (c) Representation of the same effect using a heat map, where the transport of the initial state can be observed visually

2.2 Domain wall encoding

The system described above is the one we will use for our simulations, however, as of now it is not feasible for implementation in superconducting flux qubits. The issue is that it uses a XY Heisenberg Hamiltonian, and there is not a clear way yet to recreate the XX and YY interactions with analog superconducting devices. The way to circumvent this is to change the way in which we encode the logical qubits into the physical system. The standard encoding is to associate the state of each physical spin to the state of a logical qubit. However, we can also encode the information using the so-called domain wall picture [Cha19]. The main idea, drawn from classical magnetism, is to place the qubit in the in the interface between two spins, and assign it the value $|0\rangle$ if those spins are in the same state, and $|1\rangle$, if they are on opposite states. As an example of this identification, observe the following state[3]:

$$|111000\rangle_{DW} \equiv |00100\rangle_{\text{standard}} \ . \tag{5}$$

On the right side of the identity, the '1' represents the transition between two domains of zero's and ones. Hence the name domain wall.

This encoding is perfectly applicable to the case of linear spin chains, and has already shown the ability to replicate several systems that were a priori not possible in superconducting chips [WGSE24]. The key advantage of this encoding is that since we are changing the dynamics in the physical system, we also need to change the Hamiltonian. For a large class of Heisenberg Hamiltonians in the standard picture, their domain wall equivalent only contains ZZ interaction terms. In our quantum transport case, we switch from performing the operation $|100...0\rangle \to |00...01\rangle$ to performing $|100...0\rangle \to |11...10\rangle$. Then, the Hamiltonian that achieves this result is

$$H_{DW} = + \sum_{n=1}^{N-1} t_n \sigma_n^x - J\sigma_1^z + J\sigma_N^z + \sum_{n=1}^{N-1} J\sigma_n^z \sigma_{n+1}^z. \tag{6}$$

This expression comes from considering a chain of spins containing domain walls, and constrained by a strong ferromagnetic coupling J. The $-J\sigma_1^z$ and $J\sigma_N^z$ represent on-site energies, similar to coupling the ends of the chain to fixed, virtual qubits. The opposite signs guarantee that there is at least one domain wall, corresponding to one excitation in the chain. The strength of the coupling is extremely relevant, since the map between the Heisenberg model from (2) and (6) is only exact for $|J \to \infty|$, and a finite J is only an approximation. In this Ising model, large ZZ terms prevent the creation or destruction of domain walls, conserving the number of excitations. Under this conditions, the system evolves in the subspace with a constant excitation number M. In other words, the dynamics are restricted to domain walls moving left and right. Finally, the dynamics are added through the tranverse field terms proportional to σ_n^x. These introduce movement of the domain walls along the chain, and contain the same mirror symmetry from (3), relevant to our problem. The transverse terms can also create or destroy domain walls, but this effect is suppressed when the domain wall coupling is large ($|J| \gg \lambda$). In short, this system is equivalent to fermions moving in a linear chain. The further addition of particle interactions leads to Next-Nearest-Neighbour terms in the domain wall Hamiltonian, of the form $\sigma_n^z \sigma_{n+2}^z$. However, the model we are working with is much simpler and doesn't require such terms.

[3] For a visual example of the domain wall states, see diagrams in Section 3.1.

3 State transfer with domain walls

3.1 One-qubit transport

This section describes the step-by-step implementation of the state transfer protocol using domain walls. We will start from the simpler one-qubit state case, and then extend it to more complex systems. All the numerical results have been obtained using the QuTip library in Python [LGM+24]. A detailed description of the simulation procedure can be found in Appendix A.

Let $|\psi\rangle_1$ be an arbitrary state of the first spin in the chain, $|\psi\rangle_1 = \alpha|0\rangle + \beta|1\rangle$. The rest of the spins are in the state $|0\rangle$. Then the state of the whole chain is

$$|\psi(0)\rangle = \alpha|100...00\rangle + \beta|000...00\rangle. \tag{7}$$

As mentioned above, the objective of the transport is to move the state of the first qubit to the last one, so that the final state after time τ is

$$|\psi(\tau)\rangle = \alpha|000...01\rangle + \beta|000...00\rangle. \tag{8}$$

In the domain wall picture, the evolution of the system will go from

$$|\psi(0)\rangle = \alpha|100...00\rangle + \beta|000...00\rangle \tag{9}$$

to

$$|\psi(\tau)\rangle = e^{i\tau\phi_\alpha}\alpha|11...10\rangle + e^{i\tau\phi_\beta}\beta|00...00\rangle. \tag{10}$$

In the final state, all qubits except for the last one are in the state $|1\rangle$, meaning that the state of the logical qubits in their interface between qubits $N-1$ and N is $|1\rangle$. Effectively, the initial excitation has moved to the end of the chain. There is also the presence of additional phases coming from an energy offset between the Heisenberg Hamiltonian and the domain wall Hamiltonian, which is proportional to J. Its precise form for the projection of the Hamiltonians into the M excitation subspace is

$$H_{DW}^{(M)} - H_{\text{Fermi}}^{(M)} = J(N-2M)\mathbb{I}^{(M)}. \tag{11}$$

This means that for the superposition above, there is a global phase $\phi_{glob} = JN\tau$ as well as a relative phase $\phi_{rel} = -2J\tau$. This relative phase will have to be taken into account when making measurements. However, since it is a known quantity, it can be corrected after making a measurement of the qubits. We will rewrite (12) like

$$|\psi(\tau)\rangle = e^{iJN\tau}\left(e^{-i2J\tau}\alpha|11...10\rangle + \beta|00...00\rangle\right) \tag{12}$$

The Hamiltonian from (6) is the naive translation of the state transfer problem Hamiltonian (2). However, note that the superposition of states above are not in principle attainable by the Hamiltonian with (6). The reason are the strong ferromagnetic terms at the ends of the chain, which are represented by local z-fields. We can see a visual representation of these terms in Figure 3 which show the initial and final states of the chain, and where the black spins represent the $\pm J$ local fields at the extremes.

This means that (6) only allows us to construct the state $|1\rangle$ at the start of the chain (in other words, $\alpha = 1, \beta = 0$). So to make our protocol useful, we first need to construct the state $|0\rangle$ –with all qubits down– in order to create a superposition in the first qubit. If we are unable to create a superposition, we are effectively transporting classical information.

Figure 3: Domain wall representation of the initial state $|100000\rangle$ (left) and final state $|000001\rangle$ (right) with the Hamiltonian from (6).

We solve the restriction by removing this virtual qubit in the first spin and encoding the information into the first physical qubit, and to keep a ferromagnetic-like boundary condition we don't apply the transverse field to the first qubit, effectively preventing it from evolving. In other words, the σ_x Hamiltonian term starts from $n = 2$ instead of $n = 1$:

$$H_{\text{transport}} = +\sum_{n=2}^{N-1} t_n \sigma_n^x + J\sigma_N^z + \sum_{n=1}^{N-1} J\sigma_n^z \sigma_{n+1}^z \tag{13}$$

With this, we can transport one qubit in an arbitrary state. This new initial state is represented visually in Figure 4.

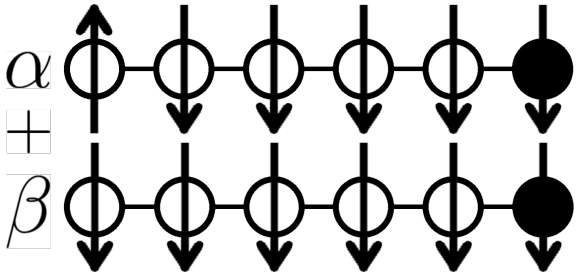

Figure 4: Domain wall representation of the state from (13) under the domain wall Hamiltonian with only one virtual qubit and no transverse field in the first physical qubit.

With this setup we can transport the state from one end to another. However a second issue arises when looking at the spins along the chain. If we compare (8) and (12), we will observe that in the domain wall final state all the qubits along the chain are entangled, that is by measuring any qubit along the chain we are able to infer the state of the rest. This does not happen in the standard picture where only the two extremes contain information about the system. This makes it so that we cannot extract the information about the phase of the state by only measuring the last qubit. However this can be solved by adding an additional step in the protocol to disentangle the chain. Essentially, we want to let it evolve in a way that all the qubits inbetween the extremes are reset to the state $|0\rangle$.

We achieve this effect by modifying the Hamiltonian after the state (12) is reached, inserting a virtual qubit in the 'down' state at the start of the chain (adding a $+J\sigma_z^1$ term through a local field), while at the same time removing the virtual qubit that we had placed initially at the end of the chain. At the same time, we also remove the transverse field in the last physical qubit. Once again, this is done to prevent it from evolving and storing the information that we had previously transported:

$$H_{\text{reset}} = +\sum_{n=1}^{N-2} t_n \sigma_n^x - J\sigma_1^z + \sum_{n=1}^{N-1} J\sigma_n^z \sigma_{n+1}^z \tag{14}$$

The end result of this operation will be that the whole chain except the last spin will "flip down" leaving us with the target state in the last qubit,

$$|\psi(2\tau)\rangle = e^{i2JN\tau}\left(e^{-i4J\tau}\alpha\,|000...01\rangle + \beta\,|000...00\rangle\right), \tag{15}$$

which is the same as (8) save for the global and relative phases. The changes in Hamiltonian and the final state can also be seen in Figures 5 and 6, including the relative phases.

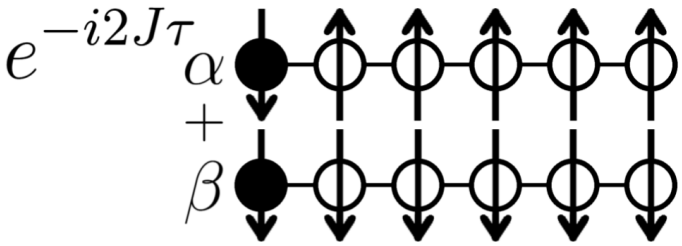

Figure 5: Change of Hamiltonian after the transport has been comlpeted, where the virtual qubit is switched to the first spin and the transverse field is removed from the last spin. The relative phase between the states is also included.

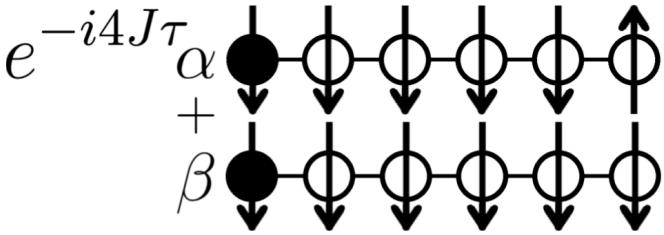

Figure 6: End result of the transport after the Hamiltonian switch, including the relative phase between the states $|1\rangle$ and $|0\rangle$.

The main cost of this operation is that we double the transfer time, since it now involves two steps. Additionally, we are forced to change the Hamiltonian and the transverse fields in the spins at a precise time (in order to preserve the mirror symmetry), which could pose a hardware challenge when implementing it. An analog example to Figure 2 showing the result of transporting the same state can be seen in Figure 7. The fidelity plot is very similar except for the small oscillations near the peak. This is due to interference from states outside the subspace of $M = 1$, and their effect is suppressed as J approaches infinity. Additionally Figures 7 highlight the difference in the chain dynamics with the Heisenberg case.

One important remark about this model is the value chosen for the Hamiltonian parameters, namely J and λ. In the standard picture λ controls the time of the simulation, but does not affect the results. However, with domain walls the exact match to the original system only happens for infinite domain wall couplings, that is $J \to \infty$. Since we have to set a finite J for the simulations, that will induce an error in the results. More specifically, the error will be controlled by the ratio J/λ, and will also depend on the length of the chain N. A more detailed analysis into these errors will be given in Section 4.1.

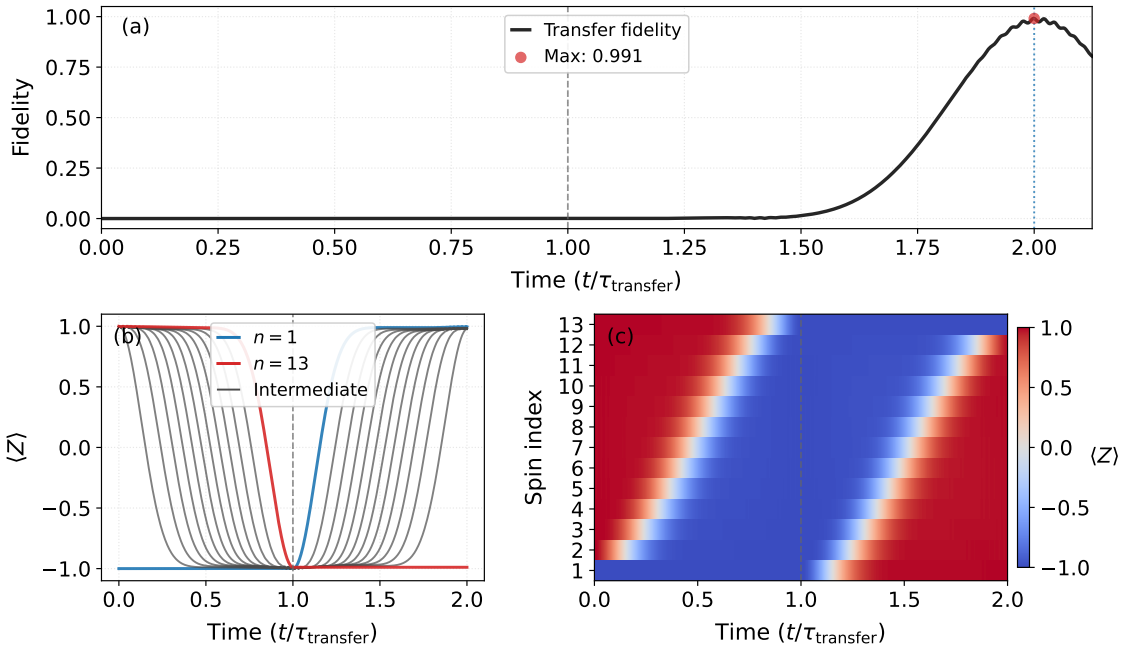

Figure 7: (a) Fidelity between the state at time t and the final expected state $|0...01\rangle$, for $N = 13$, $J = 0.5$ GHz, $\lambda = 22.72$ MHz, and initial state $|10...0\rangle$. (b) Evolution of z-component of each spin. The -1 value corresponds to the spin in the $|1\rangle$ state, and vice-versa. We can observe the swap of the initial and final spins after time τ_{transfer}. (c) Representation of the same effect using a heat map, where the transport of the initial state can be observed visually.

3.2 Multi-qubit transport

With the transport protocol established, we can extend it to states with more than one qubit. In this case we will divide the whole chain in three sections. The first and second are the registers of the sender and receiver (Alice and Bob), which will contain N physical qubits (to transport an N-qubit state). Finally, there is the wire section of the chain, which in principle can have an arbitrary length. The first phase of the transport will work in the same way, by adding a virtual qubit to the end of the chain and removing the transverse σ_x-field in the first spin. Then the state in Alice's register will evolve to form a mirror image in Bob's register. At that point, we will disable the transverse field in Bob's register and move the virtual qubit to the start of the chain, resetting all spins to the 'down' state. The only minor difference with respect to the one-qubit case is that in the resetting step the entirety of Bob's register is not affected by the transverse field. We do so to prevent those qubits from evolving. This way, the transferred state can be measured from Bob's register once the rest of the chain has been set to $|0\rangle$. Figure 8 shows the visual representation of these steps.

The same visualization steps can be taken to analyze examples of multi-qubit transfer. In this case tracking the z-magnetization becomes more confusing, since there can be ambiguity with regard to which state we are transferring/receiving by simply measuring the z-component of the spins. The most robust validation method, remains calculating the fidelity between the simulation and the expected result.

Figure 9 contains examples of 2- and 3-qubit states. We chose these states to show the capability of these chains to transfer states with and without entanglement, and with applications of interest. For example GHZ states are important for fault-tolerant quantum computing [YJ04], W states are relevant for quantum networks and interferometry

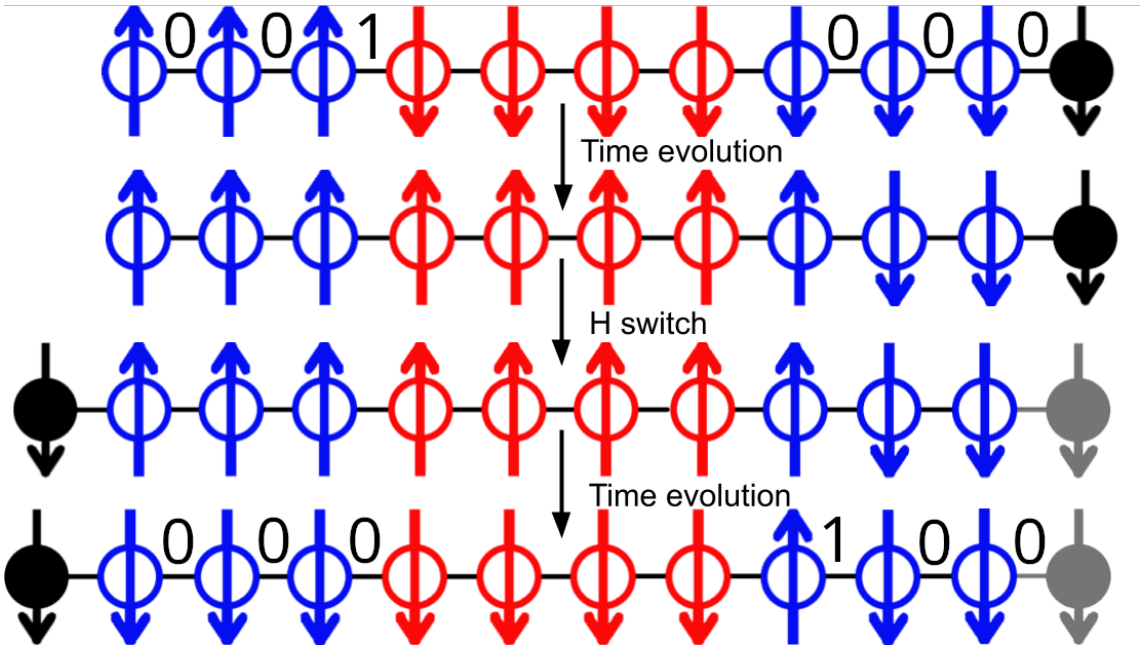

Figure 8: Example of an initial chain for the transfer of the state $|001\rangle$. The blue sections left and right represent Alice and Bob's registers respectively, and the red section represents the length of the wire. The different stages of the protocol are represented showing the changes in the virtual qubits and the results of time evolution. The grey spin at the right represents a field that does not exist anymore but is used to determine the value of the last logical qubit we measure ($|0\rangle$ if the last physical spin is down and $|1\rangle$ if it is up).

[JSW+25], and the cluster states can be used for Measurement-based Quantum computing [RBB03], or teleportation protocols [ZZXS03].

Some important observations about these results are that first we observe a drop in the overall fidelity the more qubits we transport, as well as fast oscillations that make it hard to determine the point where transfer is successful. These effects are attributed to the encoding scheme and the fact that we use a finite ZZ coupling between spins. First, this accumulates errors the more domain walls we have in the chain, and second there are phase-driven oscillations from the energy offsets that the domain wall encoding introduces. These phase differences are linear with J so they are more pronounced for large coupling strengths. This could in principle make the measurement of the qubit phases tricky as the time-window where they are correct is small. However if we account for these phases in the post-processing of the data we can mitigate their effect.

4 Error Sources and Hardware Implementation

Until now we have described a protocol for perfect state transfer. However, as we have seen in the previous section, the choice of domain wall encoding introduces errors in the transport process. Additionally, we have the aim of recreating this protocol with quantum hardware, which places restrictions to the magnitude of the different coefficients of the Hamiltonian, while simultaneously inducing additional errors. In this section we will assess the feasibility of applying these algorithms to linear chains of superconducting flux qubits by analyzing the different source of errors, and the impact they have on the result accuracy. We will first analyze in more detail the error from considering finite domain wall coupling J.

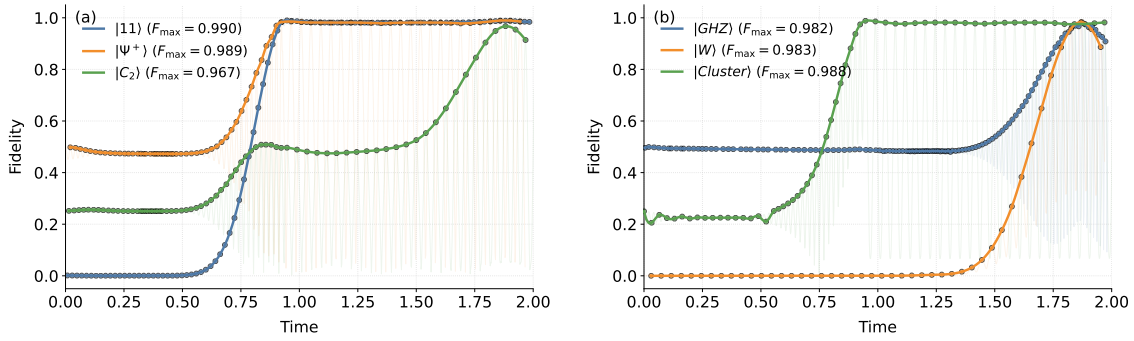

Figure 9: Fidelity for several 2-qubit states (left) and 3-qubit states (right). Fidelities have fast oscillations given by the relative phase that the energy offset from (11) introduces in states with different numbers of excitations. The peaks are marked by the dots, with interpolation lines linking them. On the left side we show the pure state $|11\rangle$ (blue), the Bell state $|\psi^+\rangle = \frac{1}{\sqrt{2}}(|11\rangle + |00\rangle)$ (orange), and the cluster state $|C_2\rangle = \frac{1}{2}(|00\rangle + |01\rangle + |10\rangle - |11\rangle)$ (green). On the right we show the following 3-qubit examples: A GHZ state, $|GHZ\rangle = \frac{1}{\sqrt{2}}(|111\rangle + |000\rangle)$ (blue), the W state $W = \frac{1}{\sqrt{3}}(|001\rangle + |010\rangle + |100\rangle)$ (orange), and another cluster state $\frac{1}{2}(|000\rangle + |011\rangle + |101\rangle - |110\rangle)$ (green).

Then we will study the errors produced by imprecise implementations of the Hamiltonian parameters and we will estimate the requirements that a superconducting device –in our case, a fluxonium qubit [MKGD09]– would need to run our algorithm.

4.1 Finite domain wall coupling

Reference [WGSE24] employs the Schrieffer-Wolf (SW) transformation [BDL11] to estimate the fidelity of the approximate domain wall Hamiltonian. This method compares the exact Hamiltonian in the spin chain picture with the domain wall one, and allows us to see their discrepancies as a function of the domain wall coupling J. Here, we will highlight the main points of the calculations, but a step-by-step derivation can be found in [WGSE24].

As mentioned in Section 3, the projections of the standard and domain wall Hamiltonians on to the subspace of M excitations differ by the energy given in (11)[4]. At the same time, we can write the general domain wall Hamiltonian H_{DW} as a function of the Fermi Hamiltonian for odd number of particles $H^{\text{odd}}_{\text{Fermi}}$ (the discussion extends to even number as well), the matrix of energy offsets from (11), denoted as D, and the off-diagonal matrix V corresponding to creation/destruction of domain walls induced by the tranverse fields in spins not adjacent to domain walls. The V term is treated as a perturbation depending on $1/|J|$.

$$H_{DW} = H^{\text{odd}}_{\text{Fermi}} + D + V \tag{16}$$

Then we find an eigenbasis for the first two terms, $H^{\text{odd}}_{\text{Fermi}} + D = U\Lambda U^\dagger$, that leaves the r.h.s of (16) as $\Lambda + \tilde{V}$, with Λ diagonal, and $\tilde{V}$ off-diagonal. With this setting we can apply the SW transformation by finding a unitary transformation e^{-S} that makes the perturbed Hamiltonian diagonal again.

This process yields a leading order correction to the domain wall Hamiltonian of $O(|J|^{-1})$. Finally, we can construct the time evolution operators for both the perturbed

[4]The general expression contains an additional term related to the NNN-interactions, that in our particular case are not present.

and unperturbed Hamiltonians, and calculate their overlap and fidelity, since this will be equivalent to the overlap between H_{DW} and H_{Fermi}. Then the fidelity between a state evolving under the effective domain wall Hamiltonian and the exact one is

$$\mathcal{F} = 1 - O(T^2|J|^{-2}). \tag{17}$$

With T being the simulation time. We can read this result in two ways. First, the fidelity decays quadratically with time. On the other hand, for a fixed time τ, such as the period of the state transfer protocol, the fidelity of the obtained state and the target state will be inversely proportional to the square of the domain wall coupling J.

On the other hand, we can see that by increasing J we can reduce the error to an arbitrary quantity. However, the physical implementation of J will be restricted by some upper bound, so at some point we will accumulate a substantial error. This however can be mitigated at the cost of a time overhead. We can see this by explicitly writing the parameter dependencies of eq. (6), that is $H_{DW}(\vec{t}, J)$, where we have denoted $\vec{t}$ as the vector of tranverse field strengths t_n from (3). Since all t_n have a constant factor λ multipling, we will take it out as $t_n = \lambda v_n$ Then, after some simulation time the Hamiltonian evolves as $e^{-iTH_{DW}(\lambda\vec{v},J)}$, and again we take the overall factor λ and obtain $e^{-i\lambda TH_{DW}(\vec{v},J/\lambda)}$. If $\lambda < 1$ with this we have essentially rescaled the domain wall coupling to a higher value at the cost of adding a time overhead.

Then, the fidelity also depends on the parameter λ such that

$$\mathcal{F} = 1 - O(T^2\lambda^2|J|^{-2}). \tag{18}$$

And consequentially, we can reduce the error by decreasing λ, so for a given error tolerance of $\epsilon = 1 - \mathcal{F}$, we can set λ to be

$$\lambda = O\left(\frac{|J|\sqrt{\epsilon}}{T}\right). \tag{19}$$

The plot of Figure 10 shows the dependence of ϵ as a function of $(\lambda/|J|)^2$, for the state $|1\rangle$. At the same time, we plot the error for the different states shown in Figure 11 As a function of $|J|/\lambda$, which will later be used to determine the desirable parameters for hardware implementation.

4.2 Robustness to hardware errors

Aside from theoretical errors, other sources are related to the hardware limitations of the devices, namely the precision with which transverse and interaction fields can be applied to the physical spins. Given that we need homogeneous J couplings, but inhomogeneous σ_x couplings with mirror symmetry, any deviation from these conditions will affect the final fidelity with the target of the state transfer. In this section we will find the limits of these errors and how they translate to the parameters of a fluxonium device. An additional factor to consider would be the qubit decoherence, and the errors induced by it. However, with the parameters chosen, our protocol has a runtime of the order of nanoseconds, very small compared to the expected coherence times of fluxonium devices. For this reason, we will only focus on coherent errors.

In general, superconducting qubits consist on a circuit made from a superconducting material that when cooled at milikelvin temperatures, exhibits a quantized energy spectrum [HWFZ20] When this spectrum is anharmonic, as obtained by including a Josephson junction [CGP24] we can access the two lowest energy levels and identify them with the

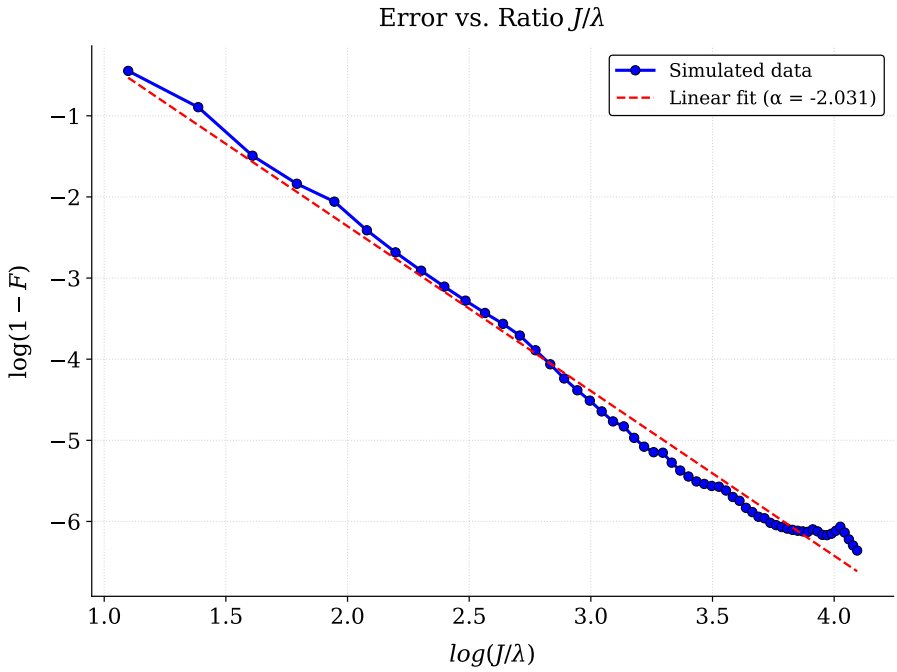

Figure 10: Error for the transport of state $|1\rangle$ as a function of J/λ in a logarithmic scale. α represents the slope of the linear fit, which confirms the qudratic dependace of (18) on the model's parameters. The points contain values of J/λ between 3 and 50. For lower numbers of the ratio, the higher order corrections to the domain wall error become large and the quadratic relation is broken.

$|0\rangle$ and $|1\rangle$ states in the computational basis. Additionally, these devices include a shunting element (e.g. a capacitor), that suppresses external noise. In a fluxonium qubit, the shunting element is a large inductance [5] formed by a chain of Josephson junctions which allows the tuning of the energy spectrum and noise suppression separately. Additionally, the fluxonium is a type of flux qubit, in which the Josephson junction and an inductance are placed in parallel and controlled by an external flux, usually denoted as ϕ_z. Finally there can be an undesired crosstalk flux, ϕ_x, that couples one qubit to another. This effect however also has to be included in the modeling of these devices. Finally, the main characteristic parameters of a fluxonium are the energies of the Josephson junction E_J, the inductor E_L, and the capacitor E_C.

Once a superconducting device has been defined, we can construct its Hamiltonian and diagonalize it to find the ground and excited states. Then the Hamiltonian can be projected into the 2-dimensional basis of these states and expressed in the Pauli basis. In our case we take the σ_z eigenstates as the persistent current states at the symmetry point $\phi_z = 0.5$[6]

From Figure 13 we can see that the ϕ_z and ϕ_x fluxes control the different components of the qubit Hamiltonian. For our quantum transfer model, the qubits need a zero σ_z term, and non-zero σ_x, which can be achieved by putting the qubit at the symmetry point ($\phi_z = 0.5$), and minimizing crosstalk ($\phi_x = 0$). However the control of these parameters will never be exact, meaning that on one hand we will get a deviation in the σ_x components, which will slightly break the mirror symmetry if (3), as well as a small undesired σ_z component, which will also alter the qubit dynamics. The last ingredient of the state

[5]The capacitive element is still present but has different roles, such as protecting from charge noise.

[6]The fluxes here are expressed in units of the magnetic flux quantum $\phi_0 = h/2e$.

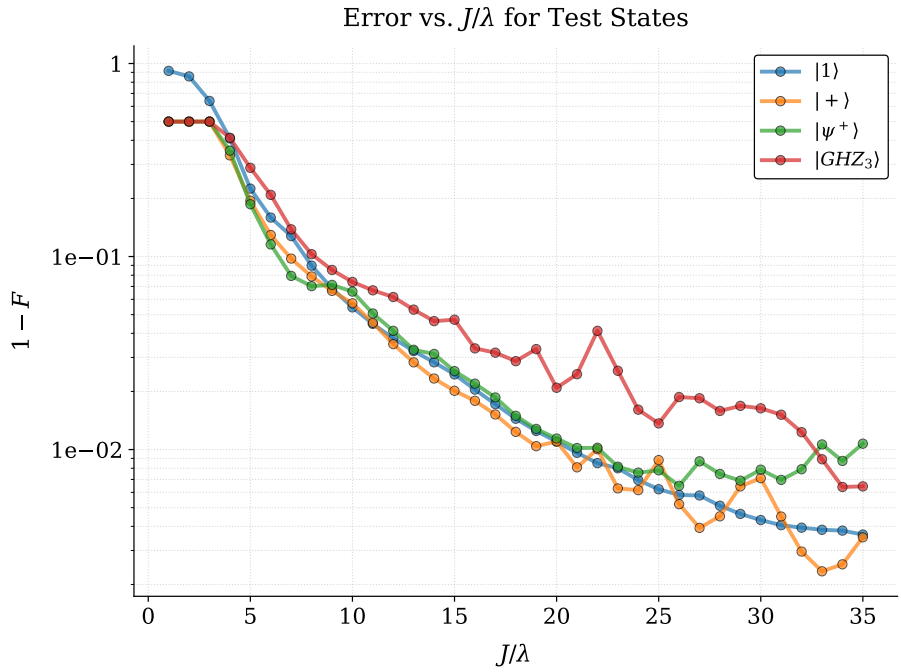

Figure 11: Simulation error as a function of the ratio J/λ for different example states.

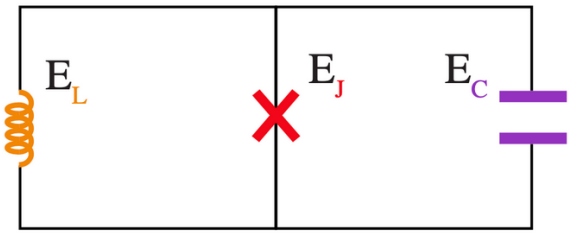

Figure 12: Simple diagram of a fluxonium qubit extracted from [LFS24]. It contains three elements in parallel: A Josephson junction (red), an inductance formed by a chain of smaller Josephson junctions (orange), and a capacitor (blue).

transfer Hamiltonian is the ZZ coupling term that is realized by considering a coupling circuit element between fluxoniums. The engineering of ZZ couplers for these devices is an area of active research with many design and hardware challenges, so a detailed description of such couplers is outside the scope of this thesis. But in short, they are also controlled by superconducting fluxes, and can be assumed to reach a maximum strength of 0.5 GHz. We can assume that the same type of errors will apply to these terms, breaking the homogeneity of the domain wall coupling strengths.

Before simulating the hardware errors we have to make a decision on the parameters of the simulation, namely N, J, and λ. From Figure 11, we observe that to achieve fidelities over 0.99 for most states, we need a ratio J/λ of at leasst 22. Then if we assume that we can produce a coupling strenght of 0.5 GHz, we set $\lambda = 22.7$ GHz, and calculate the strength of each transverse field according with (3). Finally, we model the simulation for a desired prototype consisting on $N = 13$ fluxoniums in a linear chain.

The procedure we followed to study the effect of these three sources of errors is to apply random fluctuations to the values in our simulations using a Gaussian distribution centered in the ideal values and with a variance that can be calculated as a percentage of

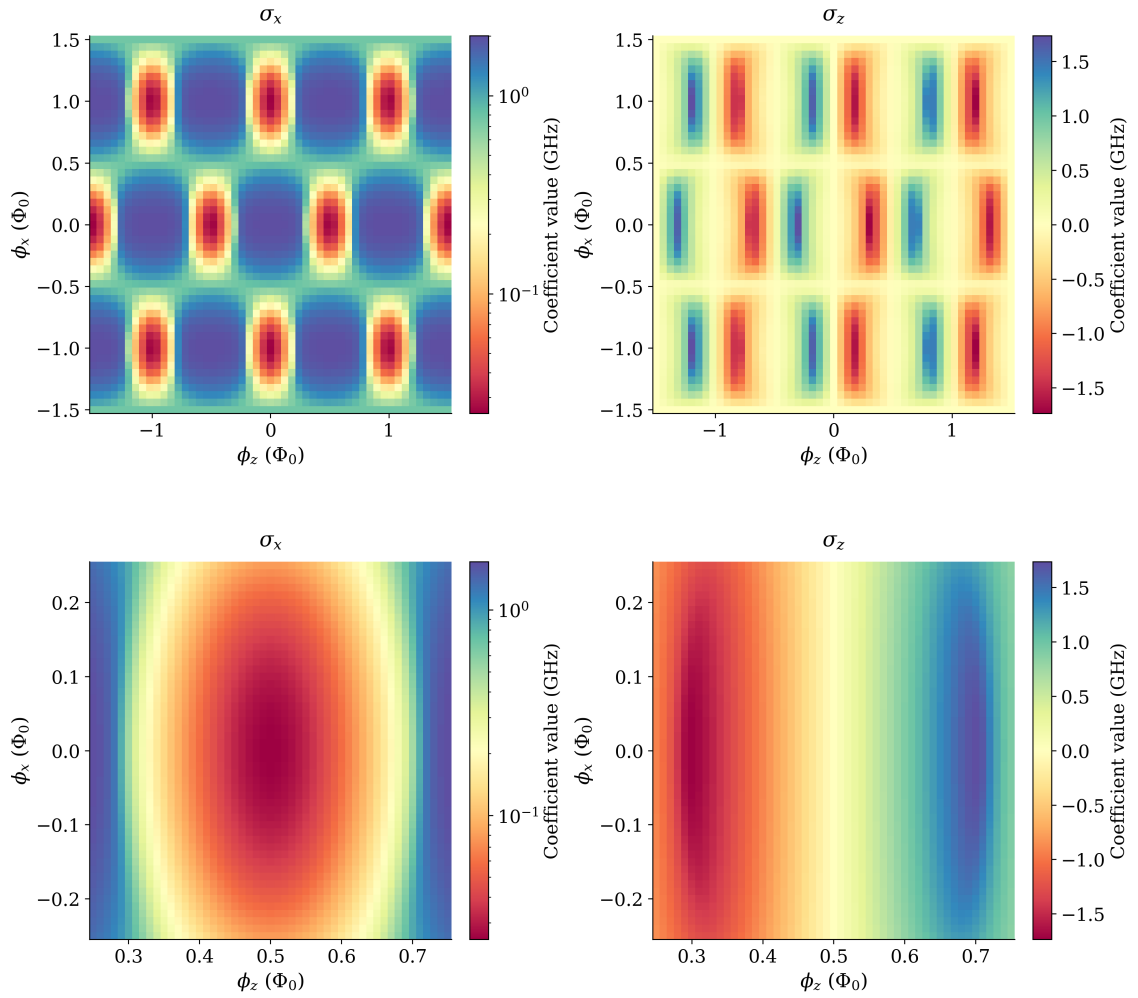

Figure 13: Effective σ_x and σ_z coefficients for a fluxonium simulated with the parameters $E_j = 4.098$ GHz, $E_l = 0.998$ GHz, and $E_c = 0.754$ GHZ, obtained from [WLZ+25]. The bottom half shows a close-up around $\phi_x = 0$ and $\phi_z = 0.5$. A minimum can be observed for both coefficients at $\phi_z = 0.5$, where the Z field disappears, and the X field takes the minimum value of 24.8 MHz, required for the transverse term of the qubit.

the mean, or fixed to a constant value for the σ_z errors, since their ideal mean is zero. We isolate the error sources one at a time and run several simulations with the same initial parameters and error variance calculating the average of the fidelities. Finally, we repeat the process for different error sizes (variances of the distribution) and plot the evolution of the average fidelities. A breakdown of each error source is shown in Figure 14. We have computed these for the transfer of the state $|1\rangle$, as it produces more accurate results.

Following the criterion of accepting results when the fidelity is above 0.9, we can determine the maximum errors that the system can admit. From the plots above, they are 7% in the transverse terms, 0.9% in the coupling terms, and between $2.5 - 3$ MHz in the Z fields. While the first source is more forgiving, the other two are pretty restrictive, and we see that a careful control of the coupler and the ϕ_z field of the qubits is required to keep the errors small. Simulations like the one from Figure 13 show that it is in theory possible to recreate the conditions for the domain wall Hamiltonians to be applied to fluxonium qubits, opening up the possibility to attempt the transfer protocol in a real device.

5 Conclusions

Or objective was to find a working quantum state transfer protocol for fluxoninium qubits with ZZ couplings, and analyzing the feasibility of applying it to real devices. First, we have presented an adaptation of a quantum state transfer protocol for linear chains of superconducting flux qubits. We began using the idea from [CDEL04], which demonstrates perfect state transfer with a Heisenberg Hamiltonian with inhomogeneous transverse fields. We avoid the use of XX and YY interaction terms –not feasible for many current superconducting architectures– by encoding the information in domain walls, inspired by the results from [WGSE24]. The result is a mapping of the exact Hamiltonian to an effective one, and it has the following properties:

- It is controlled by an additional parameter J (domain wall coupling) that equals the original Hamiltonian when taken to infinity,
- It makes use of virtual qubits in the chain ends, represented by large local Z fields, which facilitate the movement of the domain walls and prevent the creation of additional excitations.
- The protocol contains an extra step that resets the chain to the state $|0\rangle$ after the transfer is complete by switching the virtual qubits and redistributing the transverse fields, which disentangles the whole chain.
- Superpositions of states with different excitation numbers carry a known relative phase throughout the time evolution, which can be corrected after measurements.

We designed the protocol to be suitable for the transport of arbitrary superpositions of one-qubit states and multi-qubit states, and we have shown this numerically by applying it to relevant examples of up to 3-qubit states. We have validated the results by analyzing 1) the evolution of the z-component of each spin, and 2) the fidelity between the simulated chain and the theoretical expected results.

The second part of this work has been centered on the different sources of error of our protocol and determining the appropriate parameters for a hardware implementation. Our results are divided into three parts:

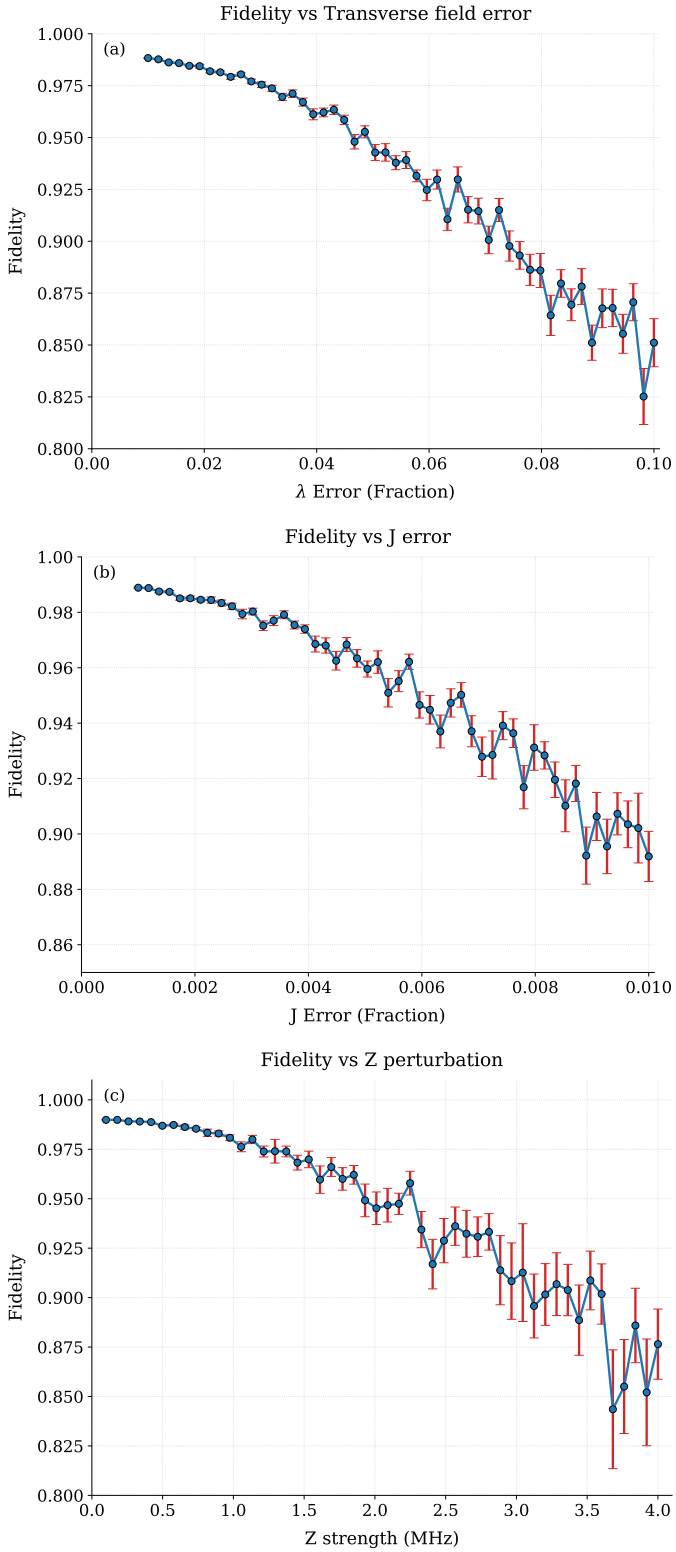

Figure 14: Evolution of the transport fidelity for $N = 13$, $J = 0.5$ GHz, and $\lambda = 22.27$ MHz with the different sources of error: Transverse fields (top), Coupling strengths (middle), and residual Z field (bottom).

1. We have analyzed the error induced by the finite domain wall coupling, which has a dependence of $|J|^{-2}$ on the fidelity. Since the construction of the Hamiltonian allows for a rescaling of the parameters, we have shown that we can mitigate the error by effectively reducing the transverse field strength while adding a time overhead. We then established a threshold for the ratio between J and the transverse field prefactor λ such that the transfer fidelity goes above 0.99.

2. We have introduced random errors to the different elements of the Hamiltonian to study the robustness of the transfer fidelity to inaccuracies in the superconducting hardware. We have determined a tolerance to a relative error of 10% to the transverse fields, and 1% to the interaction terms. Additionally, taking a maximum value of J as 0.5 GHz and a J/λ ratio of 22, we identified a tolerance to unexpected Z fields of up to 3 MHz. These results, while general, determine that superconducting devices have the ability to implement our protocol depending on the level of precision of the applied currents.

3. With the implementation into a linear chain of fluxoniums [MKGD09] in mind, we have established a potential configuration of the Josephson Junction energy, inductance, and capacitance that falls within the range of other proposed devices [WLZ+25, BDS+25].

While these results are promising, there are several next steps and alternatives to this study. First, several other protocols for perfect state transfer have been proposed [BB05, GMT09, HKC+18] which use variations of the Heisenberg Hamiltonian, albeit with additional features like time-dependent couplings, uncoupled qubits, or different chain structures. It could be of interest to rewrite such protocols in the domain wall picture and study their speed, accuracy, and error tolerance to compare them against ours. Second, while we chose to incorporate domain walls as our method for obtaining a Hamiltonian with only ZZ interactions, this approximation induces certain errors. We could consider alternative solutions and compare their impact on the total protocol error.

Finally, it would be extremely interesting to test the protocol on a real device, and analyze the actual level of control needed to implement it efficiently. This would be natural continuation of our work, however there are some challenges, including the implementation of large coupling strengths, precise control to switch the Hamiltonian at the right time, and the reconfiguration of the transverse fields in all qubits during the Hamiltonian switch, which would potentially require additional elements in the circuit design of the fluxoniums. However, if these shortcomings are solved, we could potentially have a system to transport information inside Quantum Processing Units with short transfer times and high fidelity. Another potential use would be a type of quantum repeater. This is possible because our protocol does not require the preparation of any state outside the initial one, and it includes a reset mechanism allowing the system to periodically receive states from a sender and transfer them along the chain.

Bibliography

[AAB+19] Frank Arute, Kunal Arya, Ryan Babbush, Dave Bacon, Joseph C. Bardin, Rami Barends, Rupak Biswas, Sergio Boixo, Fernando G. S. L. Brandao, David A. Buell, Brian Burkett, Yu Chen, Zijun Chen, Ben Chiaro, Roberto Collins, William Courtney, Andrew Dunsworth, Edward Farhi, Brooks Foxen, Austin Fowler, Craig Gidney, Marissa Giustina, Rob Graff, Keith Guerin, Steve Habegger, Matthew P. Harrigan, Michael J. Hartmann, Alan Ho, Markus Hoffmann, Trent Huang, Travis S. Humble, Sergei V. Isakov, Evan Jeffrey, Zhang Jiang, Dvir Kafri, Kostyantyn Kechedzhi, Julian Kelly, Paul V. Klimov, Sergey Knysh, Alexander Korotkov, Fedor Kostritsa, David Landhuis, Mike Lindmark, Erik Lucero, Dmitry Lyakh, Salvatore Mandrà, Jarrod R. McClean, Matthew McEwen, Anthony Megrant, Xiao Mi, Kristel Michielsen, Masoud Mohseni, Josh Mutus, Ofer Naaman, Matthew Neeley, Charles Neill, Murphy Yuezhen Niu, Eric Ostby, Andre Petukhov, John C. Platt, Chris Quintana, Eleanor G. Rieffel, Pedram Roushan, Nicholas C. Rubin, Daniel Sank, Kevin J. Satzinger, Vadim Smelyanskiy, Kevin J. Sung, Matthew D. Trevithick, Amit Vainsencher, Benjamin Villalonga, Theodore White, Z. Jamie Yao, Ping Yeh, Adam Zalcman, Hartmut Neven, and John M. Martinis. Quantum supremacy using a programmable superconducting processor. *Nature*, 574(7779):505–510, October 2019. Publisher: Nature Publishing Group.

[AL18] Tameem Albash and Daniel A. Lidar. Adiabatic quantum computation. *Reviews of Modern Physics*, 90(1):015002, January 2018. Publisher: American Physical Society.

[BB05] Daniel Burgarth and Sougato Bose. Conclusive and arbitrarily perfect quantum-state transfer using parallel spin-chain channels. *Physical Review A*, 71(5):052315, May 2005. Publisher: American Physical Society.

[BBD+09] H. J. Briegel, D. E. Browne, W. Dür, R. Raussendorf, and M. Van den Nest. Measurement-based quantum computation. *Nature Physics*, 5(1):19–26, January 2009. Publisher: Nature Publishing Group.

[BDG+22] Sergey Bravyi, Oliver Dial, Jay M. Gambetta, Dario Gil, and Zaira Nazario. The Future of Quantum Computing with Superconducting Qubits. *Journal of Applied Physics*, 132(16):160902, October 2022. arXiv:2209.06841 [quant-ph].

[BDL11] Sergey Bravyi, David DiVincenzo, and Daniel Loss. Schrieffer-Wolff transformation for quantum many-body systems. *Annals of Physics*, 326(10):2793–2826, October 2011. arXiv:1105.0675 [quant-ph].

[BDS+25] Gaurav Bothara, Srijita Das, Kishor V. Salunkhe, Madhavi Chand, Jay Deshmukh, Meghan P. Patankar, and R. Vijay. High-fidelity QND readout and measurement back-action in a Tantalum-based high-coherence fluxonium qubit, January 2025. arXiv:2501.16691 [quant-ph].

[BF28] M. Born and V. Fock. Beweis des Adiabatensatzes. *Zeitschrift für Physik*, 51(3):165–180, March 1928.

[Bos03] Sougato Bose. Quantum Communication through an Unmodulated Spin Chain. *Physical Review Letters*, 91(20):207901, November 2003. Publisher: American Physical Society.

[BSK+17] Hannes Bernien, Sylvain Schwartz, Alexander Keesling, Harry Levine, Ahmed Omran, Hannes Pichler, Soonwon Choi, Alexander S. Zibrov,

Manuel Endres, Markus Greiner, Vladan Vuletić, and Mikhail D. Lukin. Probing many-body dynamics on a 51-atom quantum simulator. *Nature*, 551(7682):579–584, November 2017. Publisher: Nature Publishing Group.

[Bur07] Daniel Burgarth. Quantum State Transfer with Spin Chains. May 2007.

[BV97] Ethan Bernstein and Umesh Vazirani. Quantum complexity theory. *SIAM Journal on Computing*, 26(5):1411–1473, 1997.

[CDEL04] Matthias Christandl, Nilanjana Datta, Artur Ekert, and Andrew J. Landahl. Perfect state transfer in quantum spin networks. *Physical Review Letters*, 92(18):187902, May 2004. arXiv:quant-ph/0309131.

[CGP24] Roberta Citro, Claudio Guarcello, and Sergio Pagano. *Josephson junctions, superconducting circuits, and qubit for quantum technologies*, volume 1025. 2024. arXiv:2405.20911 [cond-mat].

[Cha19] Nicholas Chancellor. Domain wall encoding of discrete variables for quantum annealing and QAOA. *Quantum Science and Technology*, 4(4):045004, August 2019. Publisher: IOP Publishing.

[CZ95] J. I. Cirac and P. Zoller. Quantum Computations with Cold Trapped Ions. *Physical Review Letters*, 74(20):4091–4094, May 1995. Publisher: American Physical Society.

[DC08] Arnab Das and Bikas K. Chakrabarti. Quantum Annealing and Analog Quantum Computation. *Reviews of Modern Physics*, 80(3):1061–1081, September 2008. arXiv:0801.2193 [quant-ph].

[FGGS00] Edward Farhi, Jeffrey Goldstone, Sam Gutmann, and Michael Sipser. Quantum Computation by Adiabatic Evolution, January 2000. arXiv:quant-ph/0001106.

[GB17] Christian Gross and Immanuel Bloch. Quantum simulations with ultracold atoms in optical lattices. *Science*, 357(6355):995–1001, September 2017. Publisher: American Association for the Advancement of Science.

[GMT09] Giulia Gualdi, Irene Marzoli, and Paolo Tombesi. Entanglement generation and perfect state transfer in ferromagnetic qubit chains. *New Journal of Physics*, 11(6):063038, June 2009. arXiv:0812.2404 [quant-ph].

[Gro96] Lov K. Grover. A fast quantum mechanical algorithm for database search, November 1996. arXiv:quant-ph/9605043.

[HKC+18] Bi-Hua Huang, Yi-Hao Kang, Ye-Hong Chen, Zhi-Cheng Shi, Jie Song, and Yan Xia. Quantum state transfer in spin chains via shortcuts to adiabaticity. *Physical Review A*, 97(1):012333, January 2018. arXiv:1801.03330 [quant-ph].

[HP25] María Hita Pérez. Design and modelization of new superconducting circuits for adiabatic quantum computation and other quantum technologies. February 2025. Publisher: Universidad Complutense de Madrid.

[HPJPGR22] María Hita-Pérez, Gabriel Jaumà, Manuel Pino, and Juan José García-Ripoll. Ultrastrong capacitive coupling of flux qubits. *Physical Review Applied*, 17(1):014028, January 2022. arXiv:2108.02549 [quant-ph].

[HRB08] H. Haeffner, C. F. Roos, and R. Blatt. Quantum computing with trapped ions. *Physics Reports*, 469(4):155–203, December 2008. arXiv:0809.4368 [quant-ph].

[HWFZ20] He-Liang Huang, Dachao Wu, Daojin Fan, and Xiaobo Zhu. Superconducting Quantum Computing: A Review. *Science China Information Sciences*, 63(8):180501, August 2020. arXiv:2006.10433 [quant-ph].

[JCZ+00] D. Jaksch, J. I. Cirac, P. Zoller, S. L. Rolston, R. Côté, and M. D. Lukin. Fast Quantum Gates for Neutral Atoms. *Physical Review Letters*, 85(10):2208–2211, September 2000. Publisher: American Physical Society.

[JSW+25] Stephen P. Jordan, Noah Shutty, Mary Wootters, Adam Zalcman, Alexander Schmidhuber, Robbie King, Sergei V. Isakov, Tanuj Khattar, and Ryan Babbush. Optimization by Decoded Quantum Interferometry, May 2025. arXiv:2408.08292 [quant-ph].

[KBDGL19] E.T. Khabiboulline, J. Borregaard, K. De Greve, and M.D. Lukin. Optical Interferometry with Quantum Networks. *Physical Review Letters*, 123(7):070504, August 2019. Publisher: American Physical Society.

[KEA+23] Youngseok Kim, Andrew Eddins, Sajant Anand, Ken Xuan Wei, Ewout van den Berg, Sami Rosenblatt, Hasan Nayfeh, Yantao Wu, Michael Zaletel, Kristan Temme, and Abhinav Kandala. Evidence for the utility of quantum computing before fault tolerance. *Nature*, 618(7965):500–505, June 2023. Publisher: Nature Publishing Group.

[KHZ+24] Milan Kornjača, Hong-Ye Hu, Chen Zhao, Jonathan Wurtz, Phillip Weinberg, Majd Hamdan, Andrii Zhdanov, Sergio H. Cantu, Hengyun Zhou, Rodrigo Araiza Bravo, Kevin Bagnall, James I. Basham, Joseph Campo, Adam Choukri, Robert DeAngelo, Paige Frederick, David Haines, Julian Hammett, Ning Hsu, Ming-Guang Hu, Florian Huber, Paul Niklas Jepsen, Ningyuan Jia, Thomas Karolyshyn, Minho Kwon, John Long, Jonathan Lopatin, Alexander Lukin, Tommaso Macrì, Ognjen Marković, Luis A. Martínez-Martínez, Xianmei Meng, Evgeny Ostroumov, David Paquette, John Robinson, Pedro Sales Rodriguez, Anshuman Singh, Nandan Sinha, Henry Thoreen, Noel Wan, Daniel Waxman-Lenz, Tak Wong, Kai-Hsin Wu, Pedro L. S. Lopes, Yuval Boger, Nathan Gemelke, Takuya Kitagawa, Alexander Keesling, Xun Gao, Alexei Bylinskii, Susanne F. Yelin, Fangli Liu, and Sheng-Tao Wang. Large-scale quantum reservoir learning with an analog quantum computer, July 2024. arXiv:2407.02553 [quant-ph].

[KLM01] E. Knill, R. Laflamme, and G. J. Milburn. A scheme for efficient quantum computation with linear optics. *Nature*, 409(6816):46–52, January 2001. Publisher: Nature Publishing Group.

[KS18] Oleksandr Kyriienko and Anders S. Sørensen. Floquet quantum simulation with superconducting qubits. *Physical Review Applied*, 9(6):064029, June 2018. arXiv:1703.04827 [quant-ph].

[KSR+22] Andrew D. King, Sei Suzuki, Jack Raymond, Alex Zucca, Trevor Lanting, Fabio Altomare, Andrew J. Berkley, Sara Ejtemaee, Emile Hoskinson, Shuiyuan Huang, Eric Ladizinsky, Allison J. R. MacDonald, Gaelen Marsden, Travis Oh, Gabriel Poulin-Lamarre, Mauricio Reis, Chris Rich, Yuki Sato, Jed D. Whittaker, Jason Yao, Richard Harris, Daniel A. Lidar, Hidetoshi Nishimori, and Mohammad H. Amin. Coherent quantum annealing in a programmable 2,000 qubit Ising chain. *Nature Physics*, 18(11):1324–1328, November 2022. Publisher: Nature Publishing Group.

[KYG+07] Jens Koch, Terri M. Yu, Jay Gambetta, A. A. Houck, D. I. Schuster, J. Majer, Alexandre Blais, M. H. Devoret, S. M. Girvin, and R. J. Schoelkopf. Charge-insensitive qubit design derived from the Cooper pair box. *Physical Review A*, 76(4):042319, October 2007. Publisher: American Physical Society.

[LFS24] Eli M. Levenson-Falk and Sadman Ahmed Shanto. A Review of Design

Concerns in Superconducting Quantum Circuits. *Qeios*, December 2024. Publisher: Qeios.

[LGM+24] Neill Lambert, Eric Giguère, Paul Menczel, Boxi Li, Patrick Hopf, Gerardo Suárez, Marc Gali, Jake Lishman, Rushiraj Gadhvi, Rochisha Agarwal, Asier Galicia, Nathan Shammah, Paul Nation, J. R. Johansson, Shahnawaz Ahmed, Simon Cross, Alexander Pitchford, and Franco Nori. Qutip 5: The quantum toolbox in python. 2024.

[Llo96] Seth Lloyd. Universal Quantum Simulators. *Science*, 273(5278):1073–1078, August 1996. Publisher: American Association for the Advancement of Science.

[LN24] David López Núñez. *Coherent Flux Qubits for Quantum Annealing*. Ph.D. Thesis, Universitat de Barcelona, April 2024. Accepted: 2024-05-10T05:59:41Z Publication Title: TDX (Tesis Doctorals en Xarxa).

[LPQ+22] Jiaqi Leng, Yuxiang Peng, Yi-Ling Qiao, Ming Lin, and Xiaodi Wu. Differentiable Analog Quantum Computing for Optimization and Control, October 2022. arXiv:2210.15812 [quant-ph].

[MKGD09] Vladimir E. Manucharyan, Jens Koch, Leonid I. Glazman, and Michel H. Devoret. Fluxonium: Single Cooper-Pair Circuit Free of Charge Offsets. *Science*, 326(5949):113–116, October 2009. Publisher: American Association for the Advancement of Science.

[MLK+16] Sreraman Muralidharan, Linshu Li, Jungsang Kim, Norbert Lütkenhaus, Mikhail D. Lukin, and Liang Jiang. Optimal architectures for long distance quantum communication. *Scientific Reports*, 6(1):20463, February 2016. Publisher: Nature Publishing Group.

[NC10] Michael A. Nielsen and Isaac L. Chuang. *Quantum Computation and Quantum Information: 10th Anniversary Edition*. December 2010. ISBN: 9780511976667 Publisher: Cambridge University Press.

[ODS+20] I. Ozfidan, C. Deng, A.Y. Smirnov, T. Lanting, R. Harris, L. Swenson, J. Whittaker, F. Altomare, M. Babcock, C. Baron, A.J. Berkley, K. Boothby, H. Christiani, P. Bunyk, C. Enderud, B. Evert, M. Hager, A. Hajda, J. Hilton, S. Huang, E. Hoskinson, M.W. Johnson, K. Jooya, E. Ladizinsky, N. Ladizinsky, R. Li, A. MacDonald, D. Marsden, G. Marsden, T. Medina, R. Molavi, R. Neufeld, M. Nissen, M. Norouzpour, T. Oh, I. Pavlov, I. Perminov, G. Poulin-Lamarre, M. Reis, T. Prescott, C. Rich, Y. Sato, G. Sterling, N. Tsai, M. Volkmann, W. Wilkinson, J. Yao, and M.H. Amin. Demonstration of a Nonstoquastic Hamiltonian in Coupled Superconducting Flux Qubits. *Physical Review Applied*, 13(3):034037, March 2020. Publisher: American Physical Society.

[OL04] Tobias J. Osborne and Noah Linden. Propagation of quantum information through a spin system. *Physical Review A*, 69(5):052315, May 2004. Publisher: American Physical Society.

[OMT+99] T. P. Orlando, J. E. Mooji, Lin Tian, Caspar H. van der Wal, L. Levitov, Seth Lloyd, and J. J. Mazo. A Superconducting Persistent Current Qubit. *Physical Review B*, 60(22):15398–15413, December 1999. arXiv:cond-mat/9908283.

[RB01] Robert Raussendorf and Hans J. Briegel. A One-Way Quantum Computer. *Physical Review Letters*, 86(22):5188–5191, May 2001. Publisher: American Physical Society.

[RBB03] R. Raussendorf, D. E. Browne, and H. J. Briegel. Measurement-based quan-

tum computation with cluster states. *Physical Review A*, 68(2):022312, August 2003. arXiv:quant-ph/0301052.

[RGL+14] Philip Richerme, Zhe-Xuan Gong, Aaron Lee, Crystal Senko, Jacob Smith, Michael Foss-Feig, Spyridon Michalakis, Alexey V. Gorshkov, and Christopher Monroe. Non-local propagation of correlations in quantum systems with long-range interactions. *Nature*, 511(7508):198–201, July 2014. Publisher: Nature Publishing Group.

[Sho94] P.W. Shor. Algorithms for quantum computation: discrete logarithms and factoring. In *Proceedings 35th Annual Symposium on Foundations of Computer Science*, pages 124–134, Santa Fe, NM, USA, 1994. IEEE Comput. Soc. Press.

[WDE+23] Karen Wintersperger, Florian Dommert, Thomas Ehmer, Andrey Hoursanov, Johannes Klepsch, Wolfgang Mauerer, Georg Reuber, Thomas Strohm, Ming Yin, and Sebastian Luber. Neutral Atom Quantum Computing Hardware: Performance and End-User Perspective. *EPJ Quantum Technology*, 10(1):32, December 2023. arXiv:2304.14360 [quant-ph].

[WGSE24] Matthias Werner, Artur García-Sáez, and Marta P. Estarellas. Quantum simulation of one-dimensional fermionic systems with Ising Hamiltonians, August 2024. arXiv:2406.06378 [quant-ph].

[WLK+05] Antoni Wojcik, Tomasz Luczak, Pawel Kurzynski, Andrzej Grudka, Tomasz Gdala, and Malgorzata Bednarska. Unmodulated spin chains as universal quantum wires. *Physical Review A*, 72(3):034303, September 2005. arXiv:quant-ph/0505097.

[WLZ+25] Fei Wang, Kannan Lu, Huijuan Zhan, Lu Ma, Feng Wu, Hantao Sun, Hao Deng, Yang Bai, Feng Bao, Xu Chang, Ran Gao, Xun Gao, Guicheng Gong, Lijuan Hu, Ruizi Hu, Honghong Ji, Xizheng Ma, Liyong Mao, Zhijun Song, Chengchun Tang, Hongcheng Wang, Tenghui Wang, Ziang Wang, Tian Xia, Hongxin Xu, Ze Zhan, Gengyan Zhang, Tao Zhou, Mengyu Zhu, Qingbin Zhu, Shasha Zhu, Xing Zhu, Yaoyun Shi, Hui-Hai Zhao, and Chunqing Deng. High coherence fluxonium manufactured with a wafer-scale uniformity process. *Physical Review Applied*, 23(4):044064, April 2025. arXiv:2405.05481 [quant-ph].

[YCY+25] Yang Yang, Robert J. Chapman, Akram Youssry, Ben Haylock, Francesco Lenzini, Mirko Lobino, and Alberto Peruzzo. Programmable quantum circuits in a large-scale photonic waveguide array. *npj Quantum Information*, 11(1):19, February 2025. Publisher: Nature Publishing Group.

[YJ04] Anocha Yimsiriwattana and Samuel J. Lomonaco Jr. Generalized GHZ States and Distributed Quantum Computing, March 2004. arXiv:quant-ph/0402148.

[YRS+22] J. Yu, J. C. Retamal, M. Sanz, E. Solano, and F. Albarrán-Arriagada. Superconducting Circuit Architecture for Digital-Analog Quantum Computing. *EPJ Quantum Technology*, 9(1):9, December 2022. arXiv:2103.15696 [quant-ph].

[ZFRC17] Erez Zohar, Alessandro Farace, Benni Reznik, and J. Ignacio Cirac. Digital quantum simulation of $\mathbb{Z}_2$ lattice gauge theories with dynamical fermionic matter. *Physical Review Letters*, 118(7):070501, February 2017. arXiv:1607.03656 [quant-ph].

[ZHY+14] Jian Zhou, Yong Hu, Zhang-qi Yin, Z. D. Wang, Shi-Liang Zhu, and Zheng-Yuan Xue. High fidelity quantum state transfer in electromechanical systems

with intermediate coupling. *Scientific Reports*, 4(1):6237, August 2014. Publisher: Nature Publishing Group.

[ZYL+25] Zheng Zhou, Zheng Yan, Changle Liu, Yan Chen, and Xue-Feng Zhang. Quantum Simulation of Two-Dimensional $\mathrm{U(1)}$ Gauge Theory in Rydberg and Rydberg-Dressed Atom Arrays. *Chinese Physics Letters*, 42(5):053705, May 2025. arXiv:2212.10863 [quant-ph].

[ZZXS03] B. Zeng, D. L. Zhou, Z. Xu, and C. P. Sun. Quantum teleportation using cluster states, April 2003. arXiv:quant-ph/0304165.

A Numerical simulation

All the numerical results in this thesis have been obtained simulating a linear chain of spins with the QuTip library in Python [LGM+24]. The state is initialized as a product state of N qubits after we pass the function a dictionary containing all the components of the state with different weights. In this initialized chain, the qubits corresponding to the sender register (Alice) contain the state that we want to send. The function also translates the state into domain walls. Similarly, we generate the target state, which is the exact result of the transport process against which we will compare our simulation.

For constructing the Hamiltonian, there are different options depending on wether we use (13), or (14). First we perform a calibration step. Since the transport time depends on the strength of the transverse fields but is independent of the state encoded, we simulate the transport of state $|1\rangle$ under (13) to determine at which exact time the domain reaches the end of the chain, and we denote it as τ_{transfer}. Then we evolve the actual state we need to transfer, again with (13), for exactly τ_{transfer}, and finally we switch the Hamiltonian to (14) and evolve it for another τ_{transfer}.

During this process, we save the evolution of the system and then run the validation functions, namely evolution of Z magnetization, and fidelity between the simulated state and the target state.

This is the structure of the core function in the algorithm:

```
1
2  def _algorithm(N, lmd, J, state_dictionary, ti, tf, Nstep):
3
4      #Hamiltonian parameters
5      Jn = J_definition(N-1, lmd)
6      tn = tn_definition(Jn)
7
8      #Generate initial and target states
9      initial_state = crate_domain_wall_state(state_dictionary)
10     target_state = create_domain_wall_target(state_dictionary)
11
12     #Initialization
13     register_length = len(initial_state.dims[0])
14     sxl, syl, szl = Initialize_Hamiltonian(N)
15
16     # CALIBRATION
17     H = Hamiltonian_forward(N, J, tn, sxl, syl, szl)
18     results_c = time_evolution(H, szl, initial_state, ti, tf, Nstep) # evolve
19     # calculate fidelity and magnetization
20     full_fidelity_c = calculate_full_fidelity(N, results_c, target_state)
21     magnetizations_c= calculate_z_expectation_values(N, initial_state,
22                                                      results_c, szl)
23     # Determine period of max fidelity
24     step_of_min_magnetization = max(int(np.argmin(magnetizations_c[:,-1])),10)
25     period = (tf - ti)*step_of_min_magnetization/Nstep
26
27     # BACK AND FORTH ALGORITHM
28     H = Hamiltonian_forward(N, J, tn, sxl, syl, szl)
29     results_f = time_evolution(H, szl, initial_state, ti, period,
```

```
                                int(step_of_min_magnetization))
    full_fidelity_f = calculate_full_fidelity(N, results_f, target_state)
    magnetizations_f = calculate_z_expectation_values(N, initial_state,
                                                      results_f, szl)
    #Redefine couplings
    Jn = J_definition(N-register_length, lmd)
    tn = tn_definition(Jn)
    # reset of the chain
    H = Hamiltonian_backward(N, register_length, J, tn, sxl, syl, szl)
    results_b = time_evolution(H, szl, results_f.states[-1] , ti, period,
                                int(step_of_min_magnetization))
    full_fidelity_b = calculate_full_fidelity(N, results_b, target_state)
    magnetizations_b = calculate_z_expectation_values(N, initial_state,
                                                      results_b, szl)

    return full_fidelity_c , full_fidelity_f, full_fidelity_b, \
           step_of_min_magnetization, period, \
           magnetizations_c, magnetizations_f, magnetizations_b

```